

The Geyser effect in the expansion of solid helium into vacuum

G. Benedek^{1,4}, P. Nieto², and J.P. Toennies^{3,a}

¹ Donostia International Physics Center, P. Lardizàbal 4, 20018 Donostia – San Sebastián, Spain

² Departamento de Física de la Materia Condensada, Universidad Autónoma de Madrid, 28049 Madrid, Spain

³ Max-Planck Institute for Dynamics and Self-Organization, Bunsenstr. 10, 37073 Göttingen, Germany

⁴ Dipartimento di Scienza dei Materiali, Università di Milano-Bicocca, Via R. Cozzi 53, 20125 Milano, Italy

Received 2 March 2010

Published online 2 July 2010 – © EDP Sciences, Società Italiana di Fisica, Springer-Verlag 2010

Abstract. The mechanism behind the intensity oscillations accompanying the flow of solid helium through a micron-sized orifice into vacuum, called the geyser effect, is investigated by measuring the pressure pulses at various locations in the entire flow system. The new results reveal that the source chamber pressure pulses have the same shape as the external detector pulses monitored in the previous experiments [G. Benedek et al., Phys. Rev. Lett. **95**, 095301 (2005)]. New experiments in which the external gas reservoir is isolated from the pressure regulator provide direct information on the mechanism of the collapse leading to the geyser pulses. Thus each geyser pulse is triggered by the breakdown of a plug located upstream of the source chamber. The flow of liquid through the orifice determines the shape of the subsequent geyser pulse.

1 Introduction

The recent interest in solid helium stems from the controversial interpretation of torsional oscillator experiments in which a decrease in the moment of inertia at temperatures below about 50 mK was attributed to supersolidity [1,2]. Although the correct explanation of these and subsequent experiments is still not clear, they have stimulated many new experiments designed to better understand the physical properties of the quantum solid. As a result, new anomalies were found in the following years in the shear modulus, in mass transport and in heat capacity measurements. Nevertheless there is still some controversy about the interpretation of the experimental results and how they are related to each other [3–5]. It is generally accepted that the origin of such anomalies are not due to superfluidity of vacancies in the ideal commensurate solid but rather must be related to other intrinsic defects such as grain boundaries or dislocations or extrinsic factors such as the ³He impurity level [6–8].

At about the same time another type of anomaly was detected in the expansion of solid ⁴He into vacuum through micron-sized orifices [9]. The flow through the orifices was observed to exhibit sharp intensity bursts with a very regular period of between a few and many hundreds of seconds. This so-called geyser effect is found only for constant source chamber pressures (P_0) and temperatures (T_0) corresponding to the solid phase. A simple kinetic theory was developed which successfully predicts the intensity pulse profiles [10]. Using available data on vacancy diffusion coefficients the observed periods were found to

be consistent with a collapse of the solid after an accumulation of vacancies into a region a few mm upstream of the aperture where the pressure gradient vanishes. It was conjectured that this region was located just before the constriction where the solid starts to accelerate towards the orifice and the source pressure takes some unspecified value P_1 .

In order to test this model and determine the source pressure over a geyser period new experiments have been undertaken in which the pressure pulses in the source chamber are measured at a position *several centimeters* upstream of the aperture. Surprisingly the pressure pulses in the source chamber were found to have nearly precisely the same time profiles as the external detector pulses measured previously. In addition, the time dependent behaviour of the pressure in the room temperature gas reservoir was also monitored. The pressure in the room temperature gas reservoir, when it is isolated from the gas supply, was found to exhibit sharp drops each of which coincided with the sharp rises of the geyser pulses. Also the source temperature exhibits a small positive glitch at each geyser pulse signalling a temporary heating. An analysis of the new data indicates that the collapse does not occur in the proximity of the orifice but in the feed line leading from the room temperature gas reservoir to the source chamber.

This report starts with a description of the modifications of the apparatus used previously. In Section 3 the source chamber pressure pulses are shown to correspond, over a wide range of temperatures, to jumps between the melting pressure and the externally applied pressure P_0 . The room temperature gas reservoir pressure drops are used to estimate the amount of material released into

^a e-mail: jtoenni@gwdg.de

the source chamber. The resulting density increase in the source chamber is found to be consistent with the pressure jump in the source chamber thereby ruling out a phase change. Thus the material remains solid during the entire pulse cycle. The rise time of the geyser pulse is measured and consistent with a rapid flow of material in the feed line leading to the source chamber. In addition small *elastic* oscillations of the pressure are also described and discussed. The implications of the new insight gained from these experiments for the theory are discussed in the final section.

2 Experimental

Figure 1 shows a schematic of the apparatus which is essentially the same as used previously [9]. In the present and the earlier experiments the source chamber has a small orifice at one end leading to the vacuum system. The orifice is a laser drilled pinhole aperture [11] with a diameter d_N of between about 2 and 5 microns and a comparable channel length. As in the previous experiments the temperature is monitored at the bottom of the cryostat with a silicon diode and a germanium resistance sensor. The temperature readings were based on the vapor pressure measured with an absolute calibrated Bourdon manometer or a calibrated gauge. The major modification with respect to the earlier experiments is the introduction of a miniature quartz piezo-electric pressure sensor (15 mm \times 5.5 mm dia.) [12], shown in Figure 1c, into the side of the source chamber 44 mm upstream of the orifice (Fig. 1b). The calibrated sensor provides relative pressures in the source chamber $P_{sc}(t)$ ¹ with a precision of $\pm 0.5\%$ and a sampling rate as high as one measurement every 10 ms (Time constant $\approx 10 \mu\text{s}$). The quartz sensors have a small linear offset, which, being linear with time, is easily accounted for. In addition a valve (A in Fig. 1a) was mounted between the gas cylinder and the external room temperature inlet. With the valve A open the pressure was stabilized at the set pressure by a pressure regulator and is referred to as P_0 . With the valve closed the pressure in the remaining gas reservoir was measured with a calibrated piezoresistive pressure gauge [13] with a precision of $\pm 0.3\%$ and sampling rate of typically one measurement every 0.5 s (Time constant $\approx 10 \mu\text{s}$). This pressure is referred to as P_{res} . Thus, in addition to the Pitot tube pressure pulses $P_{det}(t)$ of the external detector (time constant 12 ms [9]), the pressure pulses $P_{res}(t)$ and $P_{sc}(t)$ were measured synchronously. Since the pumping

¹ The pressure P_{sc} measured by the sensor is actually the stress component normal to the flow direction and may not coincide with the axial stress component P_1 defined in reference [9]. In an equilibrium elastic regime $P_{sc} = P_1 \nu / (1 - \nu)$, where ν is the Poisson ratio. Measurements with two sensors at distant positions inside the source chambers do not show any measurable pressure gradient inside the source chamber over the whole geyser period, thus suggesting that the slowly flowing solid He in the source chamber remains within a quasi-equilibrium elastic regime.

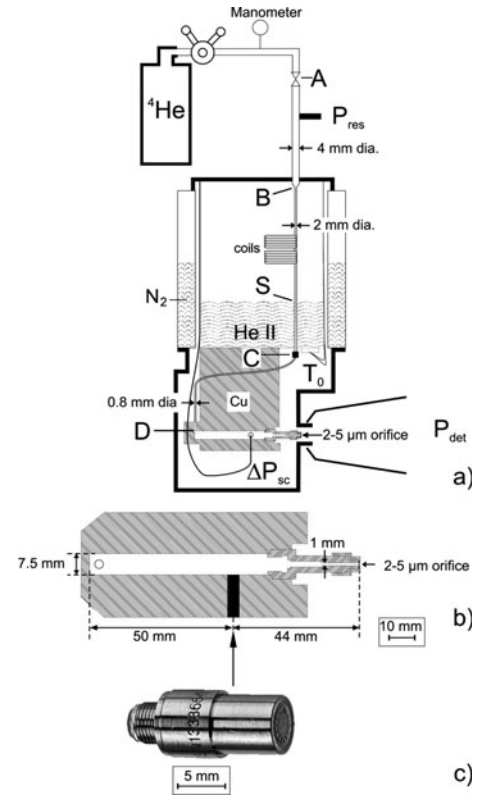


Fig. 1. (a) Schematic diagram of the gas inlet system, cryostat, feed line through the cryostat and the copper source chamber. When the valve A is closed the gas fills the volumes AB and BS, whereas the solid fills the other sections of the system in thermal contact with the cryostat, from about S to near the orifice; small liquid portions above S and close to the orifice also exist. (b) Top view cross-section of the source chamber in the Large Cell configuration. Note that the feed line entrance hole is not to scale. (c) Photograph of the quartz sensor Kistler Model 601A. The pressure sensitive end is on the right side.

speed of the two large turbo pumps ($V_p = 2760 \text{ l/s}$) in the vacuum system housing the Pitot tube detector, is constant, $P_{det}(t)$ is directly proportional to the flow speed of the liquid through the orifice

$$u_{ex} = CP_{det}, \quad C = \frac{mV_p}{kT_{det}\rho_l(0)S_N}, \quad (1)$$

where m is the He atom mass, k the Boltzmann constant, T_{det} the detector temperature, $\rho_l(0)$ the liquid beam density at the orifice and $S_N = \pi d_N^2/4$ is the orifice cross section.

In the present experiments two different cells were used as source chambers. The first one, which is called Small Cell, is the same as used previously [9]. From the feeding line end it has an internal diameter of 4 mm over a distance of 47 mm. From this point up to the aperture holder the internal diameter is increased to 7.5 mm as shown in Figure 1b (dashed line). In the Large Cell the back part of the cell has an internal diameter of 7.5 mm. Table 1 summarizes the dimensions and volumes of the inlet feed line sections and of the source chamber.

Table 1. Dimensions and volumes of the different components of the flow system. The tubing sections listed in the first column refer to Figure 1.

Part	Inner diameter d_i [mm]	Length ℓ_i [mm]	Total volume V_i [mm ³]
Tubing A-B (inlet)	4.0	200	2513
Tubing B-C ^a	2.0	3500	10996
Tubing C-D	0.8, 2.0 ^b	150	471, 2930 ^b
	4.0	47	
	6.5	1	
	7.5	12	
Small Cell	5.0	5	
in order inlet	5.6	1.7	1295
to aperture end	3.1	1.3	
	1.7	11	
	1.0	13	
	7.5	59	
	5.0	5	
Large Cell	5.6	1.7	
in order inlet	3.1	1.3	2792
to aperture end	1.7	11	
	1.0	13	

^a The inlet line B-C inside the cryostat has two 4 cm. dia. coils each with 5 windings to reduce conductive heat loss and improve the thermalization of the helium passing through the feed line.

^b Tubing C-D used in ringing experiments (Figs. 10, 11).

3 Results

3.1 Pressure oscillations in the source chamber

In the previous analysis of the geysier effect the exit velocity u_{ex} of the liquid from the orifice was assumed to correspond at any time to the solid/liquid interface pressure $P_{s/l}$. The geysier oscillations of u_{ex} around an average value \bar{u}_{ex} correspond therefore to oscillations of $P_{s/l}$ around the equilibrium melting pressure P_m . At the maximum value of $P_{s/l} = P_{s/l, max}$, occurring immediately after the collapse, it was assumed that the applied pressure P_0 of the room-temperature external gas reservoir (Fig. 1) was re-established all over the system, except in the constriction region near the orifice where $P_{s/l, max}$ was generally found to be smaller than P_0 . Moreover the actual pressure P_1 of the solid at the top of the large pressure gradient near the orifice was not identified with P_0 since no information was available about the actual pressure gradient distribution all over the system. This information is now obtained through a direct measurement of the source chamber pressure P_{sc} , which can be identified with P_1 . Figure 2 shows a typical sequence of source chamber pressure pulses measured as the cryostat was allowed to slowly heat up from 2.35 to 2.80 K at $P_0 = 63.1$ bar. The sequence of saw-tooth shaped geysier pulses is typical for these relatively high source temperatures T_0 and high pressures P_0 [9].

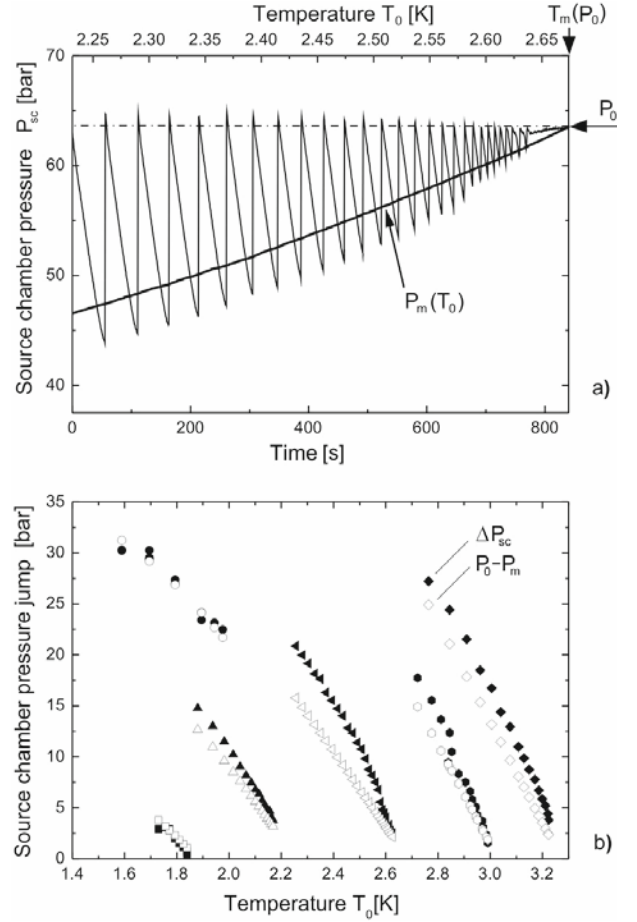


Fig. 2. (a) Large Cell source chamber pressure P_{sc} (calibrated on the external pressure $P_0 = 63.1$ bar at the melting temperature $T_m(P_0)$) versus time for a $5 \mu\text{m}$ source chamber orifice. The melting pressure P_m corresponding to the temperature T_0 is shown as a thick line. (b) Large Cell source chamber pressure jumps (solid symbols) and $P_0 - P_m(T_0)$ (hollow symbols) as functions of temperature for $P_0 = 34.1$ bar (squares), 46.8 bar (upward triangles), 58.7 bar (circles), 63.1 bar (leftward triangles), 82.2 bar (hexagons) and 94.2 bar (diamonds).

The new measurements show that the pressure oscillates in the same way as the detector pulses (see Fig. 3). To check that the pressure, though varying with time, was however the same throughout the source chamber, a second sensor was mounted at the back of the cell. The pressure jumps at the two different positions were identical to within the accuracy of the sensors. As seen in Figure 2 all the peak maxima lie within ± 1 bar of a constant value equal to the reservoir pressure P_0 . In order to calibrate the differences of pressure, the melting pressure corresponding to the measured temperature is also plotted in Figure 2a. The curve of the melting pressure $P_m(T_0)$ lies fairly close to, though in many cases slightly above, the pressure P_{sc} at the geysier minima. Thus the geysier amplitudes as measured by the sensor at the wall of the source chamber are found to be roughly equal, within about 20%, to $P_0 - P_m(T_0)$ (Fig. 2b).

Table 2. Measured relative variations over a period of $P_{det}(t)$ and $P_{sc}(t)$ for the pressures P_0 shown in Figures 3a and 3b, compared to $P_{s/l}(t)$ as derived from equation (7) at $T_0 = 1.86$ K.

P_0 [bar]	$\Delta(P_{det}^2)/P_{det,min}^2$ (expt)	$\Delta P_{sc}/P_{sc,min}$ (expt)	$\Delta P_{s/l}/P_{s/l,min}$ (Eq. (7))
35.6	0.0656	0.0755	0.0748
37.0	0.0952	0.1178	0.1086
38.0	0.1161	0.1480	0.1324
40.0	0.1553	0.2084	0.1771

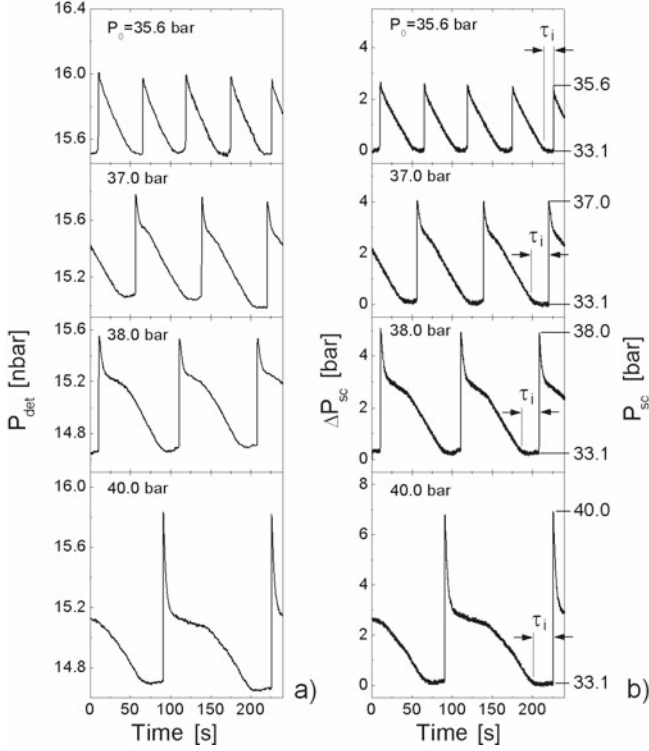


Fig. 3. Comparison between the Pitot-tube pressure P_{det} (a) and Large Cell source chamber pressure P_{sc} (b, right ordinate scale, with the maximum at P_0) and pressure variation ΔP_{sc} (b, left ordinate scale with the zero set at the melting pressure $P_m = 33.1$ bar) at $T_0 = 1.86$ K for different applied pressures P_0 , a $2 \mu\text{m}$ nozzle aperture. The time τ_i during which the pressure is constant at about P_m preceding each collapse, is called the collapse incubation time.

Figure 3 compares the simultaneously measured source chamber pulses $\Delta P_{sc}(t)$ with the external pitot tube detector pulses $P_{det}(t)$ for 4 different pressures P_0 at 1.86 K ($P_m = 33.1$ bar). All the pulse profiles in each set of measurements are virtually identical. The sharp spikes and the subsequent shoulders all have the same relative heights and shapes. Also the tails following the initial geyser spike are nearly the same. Such a close agreement in the pulse shapes indicates that the amount of material flowing through the nozzle aperture must be driven by the jump and following decay of the pressure in the source chamber. Despite the great similarity of P_{det} and P_{sc} signals, their relative variations over a period are rather different. Assuming a proportionality between u_{ex}^2 (i.e., P_{det}^2) and P_{sc} as expected for Bernoulli flow driven by the pres-

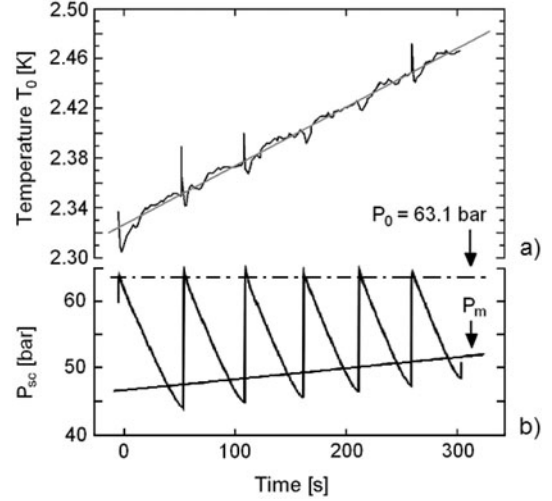


Fig. 4. The temperature ramp (a) and the corresponding source chamber geyser signal (b) during the first 300 s of the experiment shown in Figure 2a. Superimposed on the linear increase (gray straight line in (a)) the thermometer reveals sharp spikes at each geyser burst.

sure P_{sc} , the relative variations, listed in Table 2 (2nd and 3rd columns), differ by amounts ranging from 15 to 34 per cent.

3.2 Temperature oscillations accompanying the geyser pulses

The geyser pulses also produce a weak signature on the source temperature, as shown in Figure 4a for a portion of the geyser pattern of Figure 2a and reproduced in Figure 4b. The temperature signal is characterized by a very narrow positive spike (sometimes not visible) on the ms scale synchronous with the geyser burst, followed by a more prolonged dip. As discussed in the next sections each geyser pulse is associated with an influx of gas from the external reservoir into the feed line. This gas replaces the solid material which has been injected into the source chamber to bring it back up to the source pressure. Since the gas is initially close to room temperature the cryostat is momentarily heated before the gas is condensed and solidified. The subsequent downward dips, which were also seen in new experiments in which geyser pulses were observed in the flow of solid helium through narrow channels, are likely to be associated with work-flow heat absorption at the s/l interface, as discussed below.

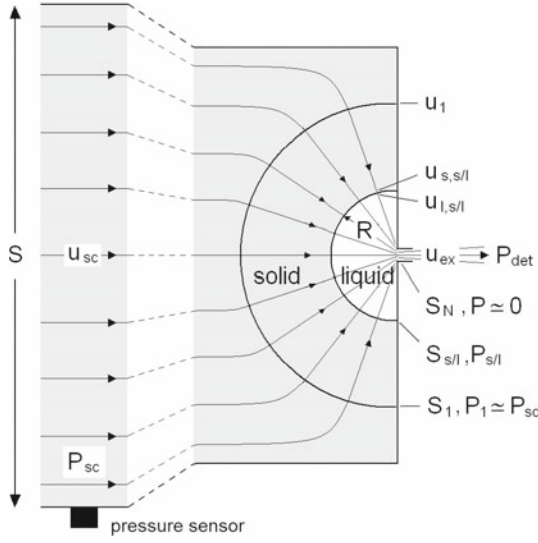


Fig. 5. (Color online) Schematic view of the solid flow in the source chamber (left) near the quartz sensor, where the flow cross section is S , the pressure P_{sc} and the flow speed u_{sc} , and near the orifice (right) of cross section S_N . In this region, starting from the surface S_1 , where the pressure is $P_1 \cong P_{sc}$, the solid flow is subject to a constriction. The consequent friction causes a pressure drop down to a value $P_{s/l}$ where the solid converts into liquid. At the solid/liquid (s/l) interface of area $S_{s/l}$ and radius R the flow velocity is suddenly raised from the solid value $u_{s,s/l}$ to the liquid value $u_{l,s/l}$ as an effect of the decrease of density. At the orifice the liquid pressure is practically zero and the exit velocity u_{ex} for a micrometric nozzle diameter is of the order of 200 m/s, to be compared with u_{sc} in the range of 10^{-4} m/s. Under conditions of constant pumping speed the detector pressure P_{det} is directly proportional to u_{ex} through equation (1).

3.3 Relationship between source-chamber pressure and detector pressure oscillations

The relationship between the exit velocity $u_{ex}(t)$, which is proportional to $P_{det}(t)$, and the source chamber pressure $P_{sc}(t)$ can be established in the quasi-stationary regime from mass and energy conservation laws. The conservation of mass (continuity) equation reads (see Fig. 5):

$$\begin{aligned} \rho_l(0)S_N u_{ex} &= \rho_s(P_{sc})S u_{sc} = \rho_s(P_{s/l})S_{s/l} u_{s,s/l} \\ &= \rho_l(P_{s/l})S_{s/l} u_{l,s/l} \equiv j, \end{aligned} \quad (2)$$

where $\rho_l(0)$ is the pressure at the orifice ($P = 0$), $\rho_s(P_{sc})$ is the pressure-dependent density of the solid, u_{sc} the flow speed in the source chamber at the sensor position, $u_{s,s/l}$ ($u_{l,s/l}$) the flow speed of the solid (liquid) at the s/l interface (where the pressure is $P_{s/l}$), j is the flux, and S is the source cylinder cross section at the sensor position. Under the non-equilibrium conditions due to the flow, and possibly to the motion of the s/l interface, $P_{s/l}$ is generally different from the melting pressure P_m .

From energy conservation we require that the power of the pressure field at the sensor position is given by $W_{in} = P_{sc}S u_{sc}$. The initial kinetic part of the power has been neglected since $u_{sc} \ll u_{ex}$. This power is equal to

the power of the emitted jet, which at zero pressure is purely kinetic, plus the power w_F dissipated by friction in the constriction region and the flow-work part w_L of the latent heat power spent at the s/l interface².

Thus:

$$P_{sc}S u_{sc} = \frac{1}{2}\rho_l(0)S_N u_{ex}^3 + w_F + w_L \quad (3)$$

The friction and latent flow-work powers, with the kinetic parts neglected, can be expressed in terms of the pressure and of the liquid and solid densities at the s/l interface as:

$$w_F = \left[\frac{P_{sc}}{\rho_s(P_{sc})} - \frac{P_{s/l}}{\rho_s(P_{s/l})} \right] j > 0, \quad (4)$$

$$w_L = -P_{s/l} \left[\frac{1}{\rho_l(P_{s/l})} - \frac{1}{\rho_s(P_{s/l})} \right] j < 0. \quad (5)$$

Since the friction power and latent work-flow power are, respectively, released to and absorbed from the thermostat, they have opposite signs. According to equation (4) the ratio $\gamma \equiv P_{s/l} \rho_s(P_{sc}) / P_{sc} \rho_s(P_{s/l})$ is ≤ 1 ; the difference $1 - \gamma$ is taken as a measure of the friction in the constriction region (Fig. 5). Although the friction term releases some heat to the cryostat, the sharp positive spike observed at each collapse in the temperature signal, Figure 4a, essentially comes from the heat released in the solidification of the inlet gas, whereas the negative deviation of the temperature signal from the linear ramp, occurring in the initial part of the period, can well be associated to the work-flow heat absorption at the s/l interface. The latter is proportional to the flow speed (Eq. (5)) and roughly reflects the shape of the corresponding geyser signal upside-down.

Substituting equations (4) and (5) into equation (3) and using equation (2), the expected Bernoulli law for the liquid phase is obtained:

$$P_{s/l} = \frac{1}{2}\rho_l(P_{s/l}) u_{ex}^2. \quad (6)$$

With equation (6) it is now possible to determine $P_{s/l}$ directly from the measured P_{det} , which is proportional to u_{ex} . The relative variations over a period of P_{sc} and $P_{s/l}$ with respect to their minimum values $P_{sc,min} \cong P_{s/l,min} \cong P_m$ are then related to the corresponding variation of P_{det} by equations (2) to (6)³. The calculation for

² The internal energy output and input terms cancel out with the internal-energy part of the latent heat provided by the cryostat and do not appear in the power balance.

³ The Geyser effect was observed in more than about one hundred measurements with temperatures T_0 ranging from 1.35 K up to 3.2 K and pressures P_0 in the solid phase up to 130 bars. Especially the new measurements at higher pressures pose a basic problem. According to equation (6) the geyser external detector oscillations imply similar oscillations of the s/l interface pressure, whereas one would expect this pressure to remain equal to the melting pressure during phenomena occurring on the time scale of seconds or minutes. In most cases the observed geyser oscillation amplitudes correspond to large

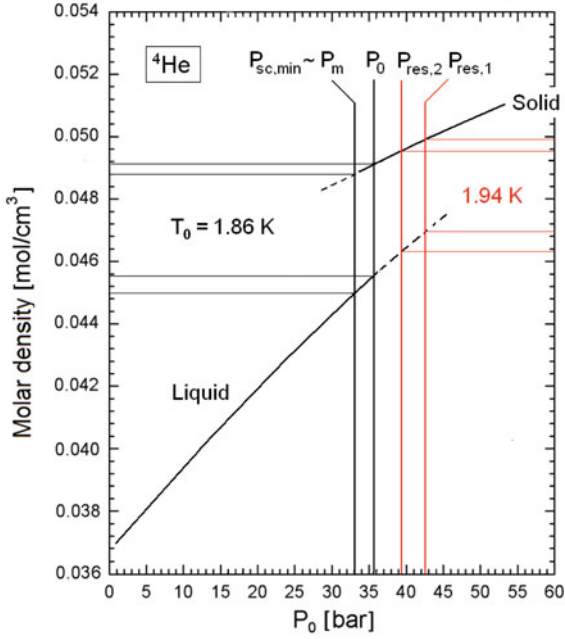


Fig. 6. (Color online) The density-phase diagram of liquid helium at $T_0 = 1.86$ K ($P_m = 33.1$ bar). The pressures $P_0 = 35.6$ bar and $P_{sc, min} = 33.1$ bar and respective molar densities corresponding to the first geyser signal of Figure 3b are indicated. For $T_0 = 1.86$ K the liquid vaporizes at $P_0 \cong 20$ mbar and the liquid molar density at the nozzle exit extrapolated to zero pressure is 0.0368 mol/cm³ [14]. The red lines correspond to one of the geyser signals at $T_0 = 1.94$ K illustrated in Figures 7 and 8, obtained with the valve closed, where the reservoir pressure drops from $P_{res, 1}$ to $P_{res, 2}$.

a constant γ gives, to first order in the variations:

$$\frac{\Delta P_{sc}}{P_{sc, min}} = \frac{\Delta P_{s/l}}{P_{s/l, min}} = \alpha \frac{\Delta(P_{det}^2)}{P_{det, min}^2}, \alpha \equiv \frac{1}{1 - P_m \beta_l} \quad (7)$$

where $\beta_l \equiv d \ln \rho_l(P_m)/dP$ is the liquid compressibility at melting. The liquid compressibility β_l is here derived from the slope of $\rho_l(P)$ in Figure 6, which gives for $P_m = 33.1$ bar (Fig. 3) a proportionality constant $\alpha = 1.140$ between the relative variations of P_{sc} and P_{det}^2 according to equation (7). This proportionality between the time dependence of the P_{sc} and P_{det}^2 signals is in perfect agreement with experiment, but the experimental value of the proportionality constant α is not the same for all P_0 (Tab. 2). It varies from 1.15 (close to the theoretical 1.140) at $P_0 = 35.6$ bar to 1.34 at $P_0 = 40.0$ bar. This deviation is attributed to an increase of the friction with P_0 .

Equation (7) also indicates that for a constant γ the relative variation of P_{sc} should be equal to that of $P_{s/l}$ and independent of γ , so that no information is obtained

deviations of $P_{s/l}$ from the nominal melting pressure P_m of the order of 17% or more at higher source pressures. Such deviations are understood as a manifestation of a non-stationary flow at the s/l interface. They imply an over-pressured liquid near the orifice during most of the period and in many cases also a slightly under-pressured solid just before collapse.

about the pressure drop $P_{sc} - P_{s/l}$ and related friction in the constriction region. Also this equality, however, is not exactly fulfilled in experiment: $\Delta P_{s/l}/P_{s/l, min}$ is systematically smaller than $\Delta P_{sc}/P_{sc, min}$, which can also be explained with a friction (positive $1 - \gamma$) which increases with $P_0 - P_m$. Correspondingly there is a pressure gradient in the constriction region (Fig. 5), which is larger for larger $P_0 - P_m$.

The simple fact that P_{sc} and, as a consequence, the pressure gradient in the vicinity of the orifice decrease with time, the latter disappearing at the collapse when $P_{sc} \sim P_m$, indicates that this pressure gradient cannot be responsible for the instability leading to the collapse. On the contrary as discussed later in Section 3.5 the pressure gradient between the reservoir and the source chamber pressure P_{sc} actually increases with time. Moreover the decrease in P_{sc} indicates that, in fact, there is virtually no flow through the inlet tube (A–D in Fig. 1) sufficient to keep P_{sc} constant during the emission (*plug model*). It is therefore concluded that the instability that causes the geyser collapse must occur upstream in the inlet tube. On the other hand the proportionality between $P_{sc}(t)$ and $P_{s/l}(t)$ (P_{det}^2) and their peculiar shape are necessarily determined by the solid flow kinetics in the constriction region between the source chamber and the s/l interface, as previously assumed in the vacancy model [9,10]. Also for the plug model an upstream drift of vacancies climbing the pressure gradient appears to be the mechanism causing the collapse of the plug. The vacancy concentration is comparatively high only close to melting, so that this condition has to be reached in order to trigger the plug collapse. This requires, however, an incubation time, to allow the vacancies to penetrate into the plug up to a critical concentration provoking the instability. In Figure 3b the incubation time τ_i is associated with the plateau preceding each collapse. Since the vacancy mobility decreases for increasing pressure, τ_i is seen to be longer for larger $P_0 - P_m$, similarly to the geyser period τ_0 .

3.4 Evidence that the helium in the source chamber remains solid and the role of vacancy induced flow

By neglecting any small inlet flow (ideal *plug model*) an upper limit on the amount of material passing through the orifice during a geyser period can be estimated and provides important information. The geyser signals in the top panel of Figure 3 for $T_0 = 1.86$ K and $P_0 = 35.6$ bar, with $P_m = 33.8$ bar, $P_{sc, min} = 33.1$ bar and a period $\tau_0 = 53.5$ s will be used for illustration. According to equation (1) the exit velocity varies between $u_{ex}(P_0) = 191.5$ m/s and $u_{ex}(P_{sc, min}) = 185.5$ m/s. With the density at the orifice exit of $\rho_l(0) = 0.0368$ mol/cm³ (Fig. 6) (nozzle of diameter $d_N = 2$ μ m) the flux calculated with equation (2) integrated over the pulse shape for an average period of 53.5 ± 1.5 s yields a total throughput of 6.89×10^{20} atoms. This evaluation has the advantage that it does not require any assumption about the state of the material in the source chamber. For the Large Cell source volume $V_{sc} = 2.792$ cm³ filled with solid and no inlet

flow, the drop in molar density (Fig. 5) from $\rho_s(P_0) = 0.04918 \text{ mol/cm}^3$ to $\rho_s(P_{sc, min}) = 0.04880 \text{ mol/cm}^3$ corresponds to the ejection of 6.39×10^{20} atoms, which is quite close to the above estimate of 6.89×10^{20} atoms. On the other hand if the solid at P_0 were to be completely converted to liquid at $P_{sc, min}$ the He molar density would drop from $\rho_s(P_0) = 0.04918$ down to $\rho_l(P_{sc, min}) = 0.04498 \text{ mol/cm}^3$ (Fig. 6). This difference corresponds to 53.8×10^{20} atoms which would leave the source chamber in the course of a geysier period. Clearly these estimates indicate that no melting of the solid occurs inside the source chamber during the geysier cycle.

The small difference between the number of ejected atoms and the number of atoms leaving the source because of the molar density decrease can be explained by a small inlet flow, equal to at most 0.5×10^{20} atoms per period. This corresponds to an average flow velocity in the CD inlet tube of only $62 \text{ } \mu\text{m/s}$ ($10 \text{ } \mu\text{m/s}$ in the BC inlet tube). Thus in a first approximation the inlet flow may be neglected during the geysier emission as if the inlet tube is completely plugged (*plug model*). On the other hand, as discussed in the next section in the closed-valve experiments the plug appears to be located upstream with the respect to D and therefore a volume $V > V_{sc}$ may contribute to the emission. An exact balance between density reduction and number of ejected atoms gives $V = 3.010 \text{ cm}^3$ and therefore the plug starts about 7 cm upstream in the CD tubing. The geysier burst can be viewed as produced by a sudden collapse of the plug as a consequence of the large pressure gradient across the plug and the resulting infiltration of vacancies into the plug volume. This view is adopted in the next subsections illustrating the plug formation kinetics and collapse mechanism.

The upstream motion of vacancies climbing the pressure gradient and the corresponding flow of atoms downstream constitutes a flow of its own, superimposed on the slow flow of the bulk solid following the geysier collapse. Such a *two-flow* mechanism rests on the observation, reported in reference [9], that the geysier period tends to zero for $P_0 \rightarrow P_m$ as $(P_0 - P_m)^{1/2}$. According to the plug model the vacancy flux entering into the source chamber $j_v(P_{sc})$ contributes to the decreased rate of P_{sc} through the vacancy density ρ_v as

$$-\frac{V}{S}\rho_v\beta_s\frac{dP_{sc}}{dt} = j_v(P_{sc}) \text{ or } dt = -\frac{V}{S}\rho_v\beta_s\frac{dP_{sc}}{j_v(P_{sc})}. \quad (8)$$

Integrating over a period τ_0 gives,

$$\tau_0 = \frac{V}{S} \int_{P_m}^{P_0} \frac{dP}{j_v(P)} \rho_v\beta_s, \quad (9)$$

where $P_{sc, min}$ has been replaced by P_m since the behavior for $P_0 \rightarrow P_m$ is of interest. Setting $\tau_0 = c(P_0 - P_m)^{1/2}$ (with, e.g., $c = 67.08 \text{ s/bar}^{1/2}$ at $T_0 = 1.85 \text{ K}$ and $41.08 \text{ s/bar}^{1/2}$ at $T_0 = 2.17 \text{ K}$ [9]), and taking the derivative of equation (9) with respect to P_0 , the vacancy flux

is given by

$$j_v(P_0) = \frac{2V\rho_v\beta_s}{Sc} (P_0 - P_m)^{1/2} = \frac{2V\rho_v\beta_s}{Sc^2} \tau_0. \quad (10)$$

Thus the vacancy flux, which is proportional to τ_0 , vanishes when the pressure has dropped below P_m unlike the bulk flow, which still remains finite at about P_m . The proportionality of $j_v(P_0)$ to τ_0 suggests that this extra flux determines the geysier period and obeys the Bernoulli law via the proportionality to $(P_0 - P_m)^{1/2}$. Such an apparently frictionless flow of mass, occurring at least near melting conditions, correlates well with the observed approximate Bernoulli regime linking, through equations (6) and (7), the exit flow velocity to the source pressure P_{sc} . In references [9,10] it was assumed that the vacancy flow was restricted to the constriction near the orifice, but the present measurements suggest that vacancies generated in the bulk solid by the decrease of pressure, will also climb the pressure gradient in the feeding line thus causing, after a time τ_0 , the collapse of the plug.

3.5 Closed-valve experiments

A direct confirmation of the plug model and the description of the plug formation kinetics are obtained from the gas reservoir pressure P_{res} when simultaneously measured with $P_{sc}(t)$ and $P_{det}(t)$. Figure 7 shows a typical measurement in which the time dependence of the reservoir pressure is compared with the simultaneously measured source chamber and detector pressure pulses before and after the valve A was closed at time $t \approx 150 \text{ s}$. Prior to the closing of the valve, small downward dips are seen in the reservoir pressure. These are attributed to the temporary removal of gas from the reservoir region in a time which is short compared to the response time of the pressure regulator. This explains the sharp spikes in the derivative curve indicated by the dotted line curve at the bottom of Figure 7a. These spikes also correlate nicely with the sharp temperature spikes in Figure 4. After closing the valve A, the gas in the feed line is cut off from the supply line and the pressure regulator. Thus with each geysier pulse gas is discharged from the feed line region between valve A and the liquid helium level inside the cryostat (S) to replace the solid material which has been released into the source chamber. As a result the reservoir pressure $P_{res}(t)$ drops from $P_{res, 1}$ to $P_{res, 2}$ (Fig. 7a) while at the same time the pressure in the source chamber P_{sc} first jumps in a few milliseconds from $P_{sc, min}$ to $P_{res, 1}$, then relaxes back to $P_{sc, min}$, etc. (Fig. 7b). The pressure difference $P_{res}(t) - P_{sc}(t)$ at the extremities of the inlet tube (Fig. 8b), as derived from $P_{res}(t)$ and $P_{sc}(t)$ plotted on the same ordinate scale for a given period (Fig. 8a), rapidly grows with time. Simultaneously $-dP_{res}/dt$ drops to zero with equal rapidity. Since the latter, for an ideal gas filling the reservoir, is proportional to the flux $-dN_{res}/dt$ (number of atoms per unit time), a decreasing flow under an increase of the pressure difference indicates the formation of a plug somewhere in the inlet tube. This once more confirms the assumption

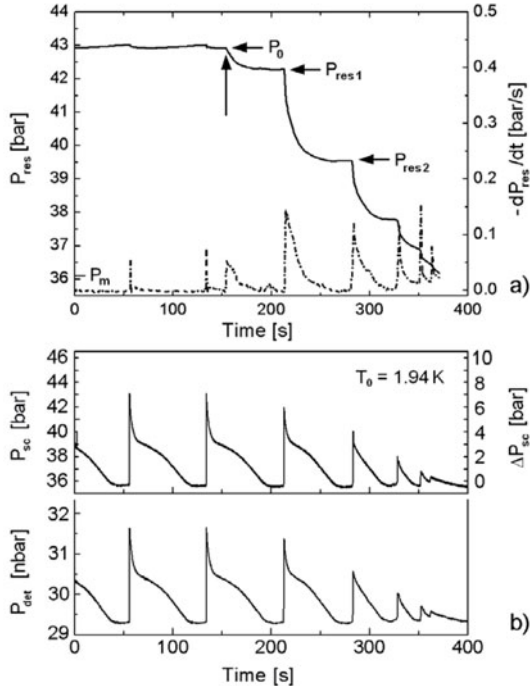


Fig. 7. (a) Pressure of the room temperature gas reservoir P_{res} as a function of time starting at $P_0 = 43.5$ bar before and after the valve A is closed at 150 s (vertical arrow). The source chamber is the Small Cell with a $2 \mu\text{m}$ orifice at $T_0 = 1.94$ K ($P_m = 36.1$ bar). After the valve is closed P_{res} drops down with each geyser pulse and forms a plateau for some time before the next collapse occurs. The dotted line curve in the bottom part of panel (a) shows the derivative of the $P_{res}(t)$ curve. (b) The simultaneously measured source chamber pressure $P_{sc}(t)$ and Pitot-tube detector pressure $P_{det}(t)$ are in phase with the derivative curve and very similar to both once the valve is closed.

made earlier that the geyser kinetics must be entirely determined by the solid flow between the source chamber and the s/l interface.

The amount of material ejected during the first drop off from $P_{res,1}$ to $P_{res,2}$ in Figures 7a and 8a is calculated by integrating $P_{det}(t)$, Figure 7b, over the corresponding period of 72 s, and is found to be 10.1×10^{20} atoms (0.0017 moles). This emission exceeds the number of atoms (6.08×10^{20}) provided by the decrease of the solid molar density inside the Small-Cell volume ($V_{sc} = 1.295 \text{ cm}^3$). This is expected since, as seen in Figure 8a, the plug is not formed instantaneously and some flow persists in the feeding line providing the missing atoms until the plug is re-established. Unlike the open-valve experiment, in the closed valve case the solid density of the column above the plug becomes less with each collapse and correspondingly fewer atoms have to be carried away during the plug formation. The closed-valve situation is schematically illustrated in Figure 9, where the pressure inside the system is plotted as a function of the tube volume. The position of the plug is signaled by a stepwise pressure drop. Since the plug is located somewhere in the inlet tubing the solid involved in the vacuum expansion in

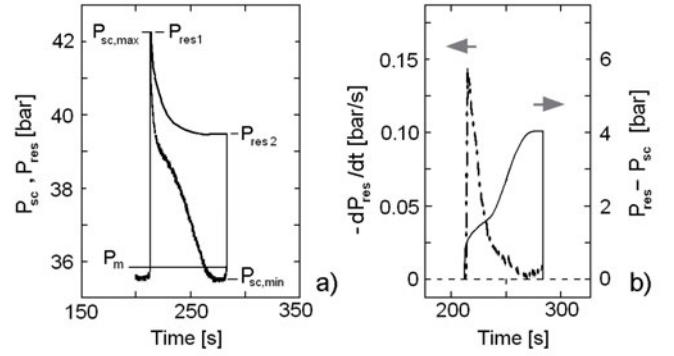


Fig. 8. (a) The reservoir and source chamber pressures, $P_{res}(t)$ and $P_{sc}(t)$ of Figure 7 are plotted on the same pressure scale over one period. (b) Comparison of the difference (r.h. ordinate scale) with the reservoir pressure derivative $-dP_{res}/dt$ (l.h. ordinate scale). For an ideal gas filling the reservoir, the derivative is proportional to the flux (number of atoms per unit time) leaving the reservoir. A decrease in flux while the “driving” pressure is increasing indicates the formation of a plug in the inlet tube.

the case of the closed valve experiment also has a volume $V \geq V_{sc}$.

In Figure 9 the collapse is represented as a rapid shift $S \rightarrow S'$ of the solid column above the plug so as to bring the whole solid to the same pressure $P_{sc,max,1} = P_{res,1}$ ⁴. After the collapse the plug is gradually rebuilt through the solidification of part of the gas until the volume SS' is refilled; correspondingly the reservoir pressure is reduced from $P_{res,1}$ to $P_{res,2}$. In the meantime the geyser emission produces a decrease of the source pressure down to $P_{sc,min} \cong P_m$ until the following collapse brings P_{sc} back to a new maximum $P_{sc,max,2} = P_{res,2}$, and so on. For simplicity $P_{sc,min}$, which has slightly different values at each collapse, is hereafter identified with P_m . As noticed above, in closed-valve experiments the decrease in P_{res} implies a stepwise decrease of the solid density in the whole column above the plug; thus the emission is not just due to the decrease of density from $\rho_s(P_{sc,max})$ to $\rho_{s,m} \equiv \rho_s(P_m)$ in the volume V but also to the density decrease in the column above the plug. The number of ejected atoms ΔN_{ex} over a period between times t_1^- and t_2^- immediately preceding two subsequent collapses at pressures $P_{res,1}$ and $P_{res,2}$, respectively, can be expressed by

$$\Delta N_{ex} = \Delta N_{res} + (\rho_{s,1} - \rho_{s,2})(V_s - V). \quad (11)$$

Here

$$\Delta N_{res} = (P_{res,1} - P_{res,2})V_{res}/kT_{res} \quad (12)$$

is the change in the reservoir atom number at temperature T_{res} , V_{res} is the reservoir volume and V_s is the total volume of the solid, with the simplified notations $\rho_{s,1} \equiv \rho_s(P_{res,1})$, $\rho_{s,2} \equiv \rho_s(P_{res,2})$. The volume of solid ΔV_s between S and S' displaced by the collapse produces a compression of the source chamber volume and

⁴ The small increase of V_{res} due to sudden motion of the plug yields a negligible decrease of the reservoir gas pressure.

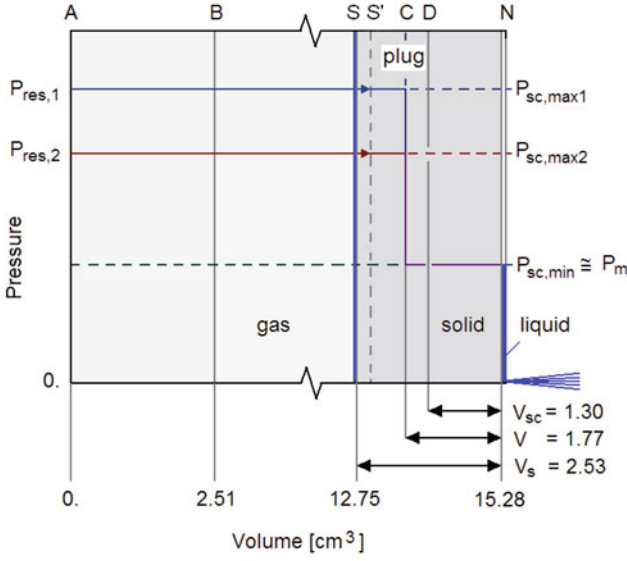


Fig. 9. (Color online) Schematic pressure distribution in the system as a function of the tubing volume (see Fig. 1 and Tab. 1) starting from the valve A (closed), when the pressure of the reservoir (AB + BS) is $P_{res,1}$ (dark blue line) or $P_{res,2}$ (dark red line) (see Figs. 7 and 8). The reservoir contains He gas at room temperature, whereas the feeding line SC + CD (see Fig. 1 and Tab. 1) and the Small-Cell source DN are filled with solid He. In the ideal-plug model and just before the collapse the pressure changes stepwise from the reservoir pressure down to a pressure close to the melting pressure P_m at the plug position in the feeding line. The analysis indicates that the plug is near the constriction point C. The collapse consists in a rapid shift $S \rightarrow S'$ of the solid column above the plug so as to bring the whole solid to the same pressure ($P_{sc,max,1} = P_{res,1}$). After the collapse the plug is reformed through the solidification of part of the gas, so as to refill the volume SS' , and a reduction of the reservoir pressure from $P_{res,1}$ to $P_{res,2}$, while the geysier emission produces a decrease of the source pressure down to P_m . With the subsequent collapse P_{sc} is quickly raised to $P_{sc,max,2} = P_{res,2}$, etc. For clarity S, S' and plug positions are not in scale, whereas A, B, C, D and N positions are in scale according to Table 1 (Small-Cell).

a density increase $\rho_{s,m} \rightarrow \rho_{s,1}$, so that $\Delta V_s = (1 - \rho_{s,m}/\rho_{s,1})V$. This volume is then refilled by the solidification of the same number of atoms lost within a geysier pulse (Eq. (12)):

$$\Delta N_{res} = \rho_{s,2} \Delta V_s = \rho_{s,2} (1 - \rho_{s,m}/\rho_{s,1}) V. \quad (13)$$

Thus equation (11) becomes (to first order in the small density changes):

$$\Delta N_{ex} = (\rho_{s,1} - \rho_{s,m})V + (\rho_{s,1} - \rho_{s,2})(V_s - V). \quad (14)$$

This form of the continuity equation encompasses both open-valve and closed-valve experiments. In the *open-valve* case identical conditions are recovered after each period ($\rho_{s,1} = \rho_{s,2} = \rho_s(P_{sc,max})$) and only the first term survives in equation (14): the emission is exclusively due to the density decrease inside the volume V , as already

stated in Section 3.5. As seen for the open-valve experiments of Figure 3 the volume V can be to a good approximation identified with the source cell volume V_{sc} . In the *closed-valve* case the emission is due to both terms of equation (14), produced by the change in the solid density below and above the plug position. Here one can define an *effective source volume* V^* so that $\Delta N_{ex} = (\rho_{s,1} - \rho_{s,m})V^*$. From equation (14)

$$V^* = V + \frac{\rho_{s,1} - \rho_{s,2}}{\rho_{s,1} - \rho_{s,m}}(V_s - V). \quad (15)$$

Experiment gives $V^* = 2.15 \text{ cm}^3$. The closed-valve sequence of geysier bursts (Fig. 7) can be described starting from equations (12) and (13) with the density changes expressed through the corresponding pressure changes. By approximating the n -th reservoir pressure jump as $P_{res,n} - P_{res,n+1} \cong -\partial P_{res,n}/\partial n$ and integrating one finds

$$P_{res,n} - P_m = (P_{res,1} - P_m) e^{-\kappa n}, \quad \kappa \equiv kT_{res} \rho_{s,m} \beta_s V / V_{res}. \quad (16)$$

Then, from the approximate proportionality between the n -th geysier emission ($\Delta N_{ex})_n$ and its period τ_n (assuming a constant V^*) it is found that

$$\frac{\tau_{n+1}}{\tau_n} = \frac{P_{res,n+1} - P_m}{P_{res,n} - P_m} = e^{-\kappa}. \quad (17)$$

The proportionality between the geysier periods (τ_n) and amplitudes ($P_{res,n} - P_m$) explains the apparent *self-similarity* of the decaying closed-valve sequence of geysier bursts⁵.

With T_{res} at room temperature, the total Small Cell system volume $V_{res} + V_s = 15.28 \text{ cm}^3$ (Tab. 1) and the densities taken from Figure 6, it is found that $V_s = 2.53 \text{ cm}^3$, $V_{res} = 12.75 \text{ cm}^3$, $\Delta V_s = 0.028 \text{ cm}^3$, and $V = 1.77 \text{ cm}^3$. This indicates that fluid He I fills a large portion of the feeding line. It is more interesting to note that V_{sc} plus the volume of the narrow inlet tube CD (0.471 cm^3 see Tab. 1) is 1.77 cm^3 , i.e., $\cong V$, which strongly suggests that the *plug forms at the constriction point C*. Moreover from equation (16) $\exp(-\kappa) = 0.60$, in reasonable agreement with the experimental average amplitude ratio (0.57) and average period ratio (0.55) from one pulse to the next for the closed valve experiments. Finally, the displacement of the solid column in the tubing BC (diameter $d_{BC} = 0.2 \text{ cm}$) can be obtained from ΔV_s and is found to be $x_0 = \Delta V_s / S_{BC} = 0.9 \text{ cm}$, with $S_{BC} = \pi d_{BC}^2 / 4$. According to equation (13), ΔV_s as well as the number of atoms ejected during a period τ_0 , ΔN_{ex} are both proportional to V . Therefore under the same experimental conditions τ_0 is proportional to V . The comparison between Large-Cell and Small-Cell data shows that this proportionality is well verified. The information about the plug model obtained from the close-valve experiments is now used for a discussion of the collapse dynamics.

⁵ As shown in [9], the period deviates from linearity with pressure near P_m and vanishes for $P_0 \rightarrow P_m$ as $(P_0 - P_m)^\gamma$ with $\gamma < 1$. This may be understood as due to an increase of the compressibility in the critical limit $P_0 \rightarrow P_m$.

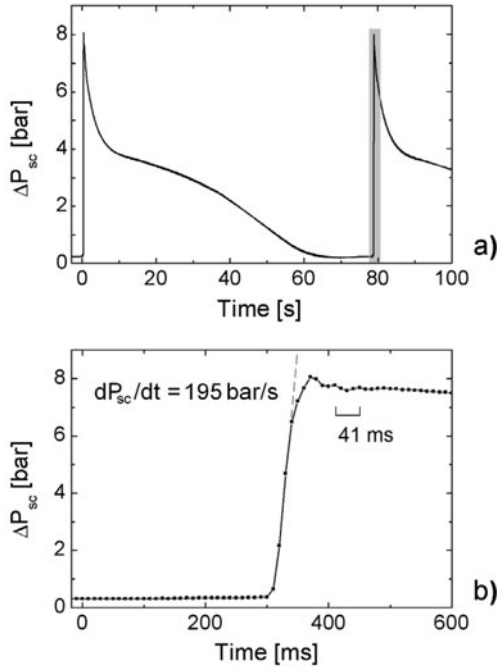


Fig. 10. (Color online) (a) Geysers pulses for $P_0 = 43.5$ bar and $T_0 = 1.94$ K (Large-Cell experiment). The ramp of a geysers burst (grey region) is shown on an enlarged time scale in (b). During the collapse the pressure rises at a speed of 195 bar/s. The collapse is followed by a small ringing with a period of 41 ms.

3.6 Collapse dynamics

The electronics of the Kistler pressure sensor mounted in the source chamber was capable of recording the pressure at a sampling rate of one point every 10 ms. Figure 10 shows a time expanded view of the initial pulse rise of a typical open-valve geysers at $P_0 = 43.5$ bar and $T_0 = 1.94$ K (Large-Cell source chamber). The initial rise corresponds to a rate of 195 bar/s and the time to reach the maximum is about 40 ms. This is the time required by the solid column in the inlet tube above the plug to shift downward, as an effect of collapse. Thus the column in the tubing BC (Fig. 1) flows during the collapse at an average speed of 23 cm/s. It is noted that the collapse event is detected at the source chamber sensor with a delay given by the time for a longitudinal sound wave to cover the plug-sensor distance. For the plug located at the point C of the feeding line this distance is about 20 cm (Fig. 1 and Tab. 1), which, for a longitudinal sound speed in the solid of $v_L = 530$ m/s [15] gives an upper limit on the delay of 0.38 ms. This is much less than the time resolution of the sensor and therefore can be neglected.

The geysers signal reproduced in Figure 10b for $P_0 = 43.5$ bar and $T_0 = 1.94$ K shows, immediately after the ramp, a few tiny oscillations of about 25 Hz. Such oscillations (*ringing*) are better seen in experiments at lower pressure and temperatures, e.g., in the geysers signals, reproduced on an enlarged scale in Figure 11 measured at

$P_0 = 34$ bar for $T_0 = 1.84$ and 1.69 K. Here the oscillations have a smaller damping and a lower frequency of about 17 Hz. The ringing effect is attributed to the elastic response of the solid to the collapse and can be understood with a simple mechanical model.

The collapse due to the plug breakdown is modeled as a rapid slide of the solid He mass m contained in the feeding line pushed by the reservoir pressure P_0 against the pressure $P_{sc, min} \sim P_m$ until the latter is raised back to P_0 . It may be assumed that during this process, occurring on the millisecond scale, the amount of He ejected through the nozzle is negligible. The mechanical response of the solid is determined by an elastic constant $c_L = \rho_{s, m} M \mathbf{v}_L^2 = 553$ bar (where $M = 4$ g/mol) [16] and a kinetic sliding friction affecting the motion in the feeding line. This is taken in the form $F_s [1 + (\mathbf{v}/\mathbf{v}_0)^2]^{1/2}$ [17], where F_s is the limiting friction for the sliding velocity $v \rightarrow 0$, and v_0 is a parameter which signals the transition from the incipient kinetic regime ($v < v_0$) to the linear kinetic regime ($v \gg v_0$).

As suggested by the previous analysis, the plug is assumed to be located at the inlet of tubing CD (section S_{CD}). Thus the force acting on the column at time $t = 0$, just after the plug removal, is given by $f = P_0 S_{BC} - P_{sc, min} S_{CD}$. This is opposed during the slide by a growing elastic reaction $-kx$ of the solid mass below the plug, where x is the displacement of the column at the upper extremity (S in Fig. 9). The effective force constant $k = c_L / \sum_i V_i / S_i^2$, with the sum extending to all portions of the tubing of volume V_i and section S_i listed in Table 1, is that of the total volume of solid He ($\sum_i V_i = V_s$), since the elastic response involves the deformation of the whole solid mass. Thus only one single coordinate x describing the displacement of the column mass $m \cong \rho_{s, m} M (V_s - V_{sc})$ needs to be considered. It is assumed to obey the following equation of motion

$$m\ddot{x} = f - kx - F_s \sqrt{1 + (\dot{x}/v_0)^2} \text{sgn } \dot{x}. \quad (18)$$

This equation is seen to give a good description of the collapse kinetics and ringing in the incipient kinetic regime ($\dot{x} < v_0$), for which the factor $\text{sgn } \dot{x}$ is needed to account for the dynamic part of the friction opposing the velocity. The friction constant F_s is related to the equilibrium displacement x_0 reached after the collapse (when $\dot{x} \rightarrow 0$) by $f - F_s = x_0 k$. The source pressure change and feed-line solid column displacement during the collapse, calculated with equation (18) with the initial conditions $x(0) = 0$ and $\dot{x}(0) = 0$ for the data of Figures 11a, 11b ($P_0 - P_{sc, min} = 2.65$ bar) are shown in Figure 12a. The asymptotic displacement $x_0 = 1.5$ cm has been determined by multiplying the Small-cell value of 0.9 cm by the Large-to-Small Cell ratio of the volumes V assuming the plug at position C as for the Small-Cell closed-valve experiments. On the other hand it is not expected that the position of the interface S found for closed-valve experiments is the same in the open-valve case. It is thus preferable to fit the solid column mass, i.e., its volume $V_s - V_{sc}$, to the experimental ringing period (58 ms). Also the velocity parameter v_0 is not known and is fitted to

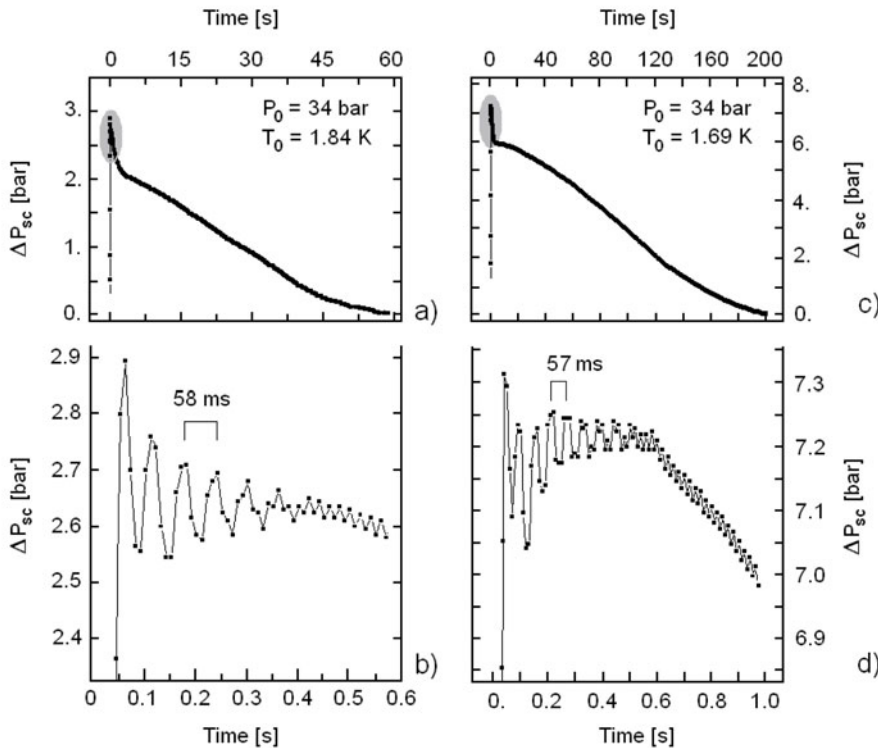


Fig. 11. Two geysier pulse profiles at $P_0 = 34$ bar and temperatures $T_0 = 1.84$ K (a) and 1.69 K (c) (Large-Cell experiments) are plotted as a function of time on the top abscissa. The bottom panels (b) and (d) show the regions marked with grey shading in (a) and (c) on an enlarged time scale which exhibit ringing oscillations (about 17 Hz) of the source chamber pressure. The residual faster (50 Hz) oscillation at longer times is noise induced by ac power supply.

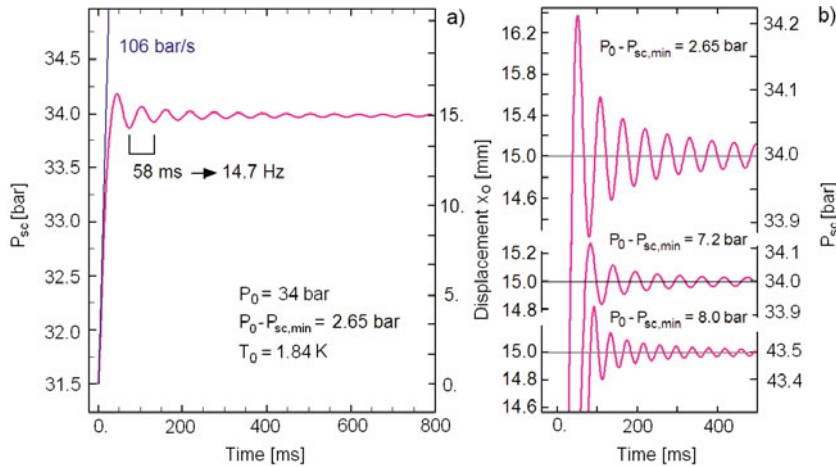


Fig. 12. (Color online) (a) The calculated pressure ringing of the source chamber pressure following the initial ramp of the geysier burst according to equation (18) (l.h. scale) and the corresponding displacement of the solid He column in the feeding line at the plug position (r.h. scale). The calculation refers to the case of Figures 11a, 11b. The period of 58 ms has been fitted to experiment. (b) Amplified ringing oscillations calculated from equation (18) for the cases of Figures 11a, 11b ($P_0 - P_{sc,min} = 2.65$ bar), Figures 11c, 11d ($P_0 - P_{sc,min} = 7.2$ bar) and Figure 10b ($P_0 - P_{sc,min} = 8.0$ bar). For sake of clarity the time origin of the latter two diagrams has been slightly shifted, the onset time, defined by the position of the first peak, being about the same for all diagrams. The calculated pressure rise speed for the three diagrams is of 106, 161 and 235 bar/s, respectively.

the first oscillation amplitude. The calculation shown in Figure 12a reproduces quite well the observed ringing pattern with a velocity parameter $v_0 = 60$ cm/s and a fairly large solid volume $V_s = 11.5$ cm³. Similar fits are made for the ringing oscillations of Figure 11d ($P_0 - P_{sc,min} = 7.2$, period = 57 ms; $v_0 = 60$ cm/s, $V_s = 11.3$ cm³) and Figure 10b ($P_0 - P_{sc,min} = 8$, period 41 ms; $v_0 = 92$ cm/s, $V_s = 8.0$ cm³). The three fits are shown on a magnified scale in Figure 12b. The corresponding predicted pressure rise speeds are 106, 161 and 235 bar/s, in qualitative agreement with the observed values. The pressure rise speeds, like the ringing frequencies (17.2 Hz, 17.5 Hz, 24.4 Hz)

and the velocity parameter v_0 , grow with the initial pressure P_0 and/or the pressure difference $P_0 - P_{sc,min}$. Quite intriguing are the fitted values of V_s , which are considerably larger than the value obtained for the Small-Cell closed-valve experiments. In the present case the interface S would be located in the upper part of the tubing BC not in contact with the cryostat liquid He. One possible explanation is that at the interface S the solid is in contact with a fairly dense He I fluid (which gradually rarifies towards A due to the rise of temperature), with a comparatively small change of acoustic impedance so that also part of the fluid column should be involved in the elastic response. On

the other hand the acoustic impedance of solid He is much smaller than that of the copper container, which ensures a complete reflection of the sound wave at the He/Cu walls. Thus the fitted values of V_s correspond to the effective volume involved in the ringing effect. Very likely the origin of the damping is the extra volume in the fluid state. It is however remarkable that also the damping is fairly well reproduced by the simulation. It may be concluded that altogether this simple model provides a qualitatively good picture of the collapse dynamics.

4 Discussion and conclusions

New measurements are reported which give new insight into the geyser phenomenon observed previously [9,10] in the expansion of solid helium through a narrow orifice into vacuum. Previously only the pulses of flux passing through the orifice were monitored via the pressure bursts in the external vacuum system. In the new experiments the pressure inside the source chamber is also measured simultaneously with the external detector pulses. The pressure in the source chamber oscillates between the externally applied pressure P_0 and a pressure which is very close to the melting pressure for the source temperature $P_m(T_0)$ with a time profile almost identical to that of the geyser jet. This indicates that the collapse leading to the geyser pulse does not occur, as previously assumed, near the orifice, but is due to the sudden collapse of a plug located somewhere upstream in the feed line. Since the plug is rapidly reformed the subsequent decrease of the pressure in the source chamber and at the external detector can only be explained by the flow of the solid within the source chamber, its melting near the orifice, and the flux of liquid through the orifice. In other words the observation of identical pressure profiles in the source chamber and in the vacuum chamber is determined by the time dependent discharge through the nozzle orifice. The total flow, however, appears to be the sum of two components: the bulk flow, constituting a finite background also in the absence of the geyser oscillations, and an apparently frictionless flow attributed to an upstream motion of vacancies, which vanishes at melting and determines the geyser period.

Also new are measurements of the pressure in the external gas reservoir when it is isolated from the pressure regulator (closed-valve experiments). With each geyser pulse the reservoir pressure exhibits a sharp drop-off with the geyser pulse sequence showing a proportional decrease in amplitude and period. The temporal behaviour of these drop-offs in relation to the source chamber pulses provides confirming evidence for plug collapse as the mechanism which initiates the geyser pulses.

In both the closed-valve and open-valve experiments each geyser pulse is initiated by a sudden release of a segment of the plug into the source chamber. This explains the sudden rise of the source chamber pressure to the pressure of the external gas reservoir. This is further confirmed by the observed rapid pressure increase in the range of 200 bar/s and pressure ringing. Both observations are explained by a simple model simulating the equation

of motion of the suddenly displaced plug segment. Both the elastic constant of the solid and the wall friction enter into the dynamics of the pressure ringing. When the solid below the plug reaches a pressure close to the melting pressure the plug is dissolved and the rapid collapse occurs.

Evidence is presented that the solid in the source chamber does not melt over the entire geyser period except in a region very close to the orifice. The formation of a liquid is not required to induce the plug collapse. Apparently the increased plasticity induced by the rapid increase of the vacancy concentration in the downstream solid at pressures somewhat below the melting conditions is sufficient to suddenly re-establish the flow in the feed line until a new plug is rapidly re-established. The peculiar shapes of the geyser pulses, which, as shown in previous papers [9,10], may change dramatically with pressure and temperature, essentially depend on the transport processes near the orifice, and will be discussed in a forthcoming theoretical paper.

It is noted that after the pressure has dropped to the melting pressure, or slightly below, the collapse generally occurs after a short delay. This incubation time, like the geyser period, is seen to increase with pressure, and is viewed as the time needed for vacancies to drift into the plug and provoke its collapse.

In summary the geyser process involves two kinetic processes. One concerns the liquid flow through the orifice originating from the flow of the vacancy saturated solid produced in the geyser collapse. This kinetics determines the characteristic shape of the fall-off of the initial pressure spike until it reaches the melting pressure. The other kinetic process concerns the formation of the plug and its break-down, both processes being associated with the increasing pressure difference between the reservoir and the source chamber. As the pressure gradient at the plug becomes large and at the melting pressure the vacancy concentration in the source chamber is dramatically increased, a massive injection of vacancies into the plug leads to the break-down. The closed-valve experiments show both kinetic processes in a single measurement and their possible interplay during the plug formation transient.

The effectiveness of the pressure equilibration was studied in further experiments where the source chamber was divided by a separating wall and connected by a micron-sized capillary. These measurements have the advantage that the geometry of the feed line and that of the orifice are identical and well defined making a more quantitative analysis possible. Depending on temperature and pressure conditions resistant and non-resistant flow through the capillary were measured. The results of these experiments will be published elsewhere [18].

The authors thank Anton Kalinin for assistance with the measurements. Giorgio Benedek acknowledges the support of the Ikerbasque Foundation (project ABSIDES), Spain. Pablo Nieto thanks to Prof. Rodolfo Miranda for financing his visits to Göttingen.

References

1. E. Kim, M.H.W. Chan, *Nature* **427**, 225 (2004)
2. E. Kim, M.H.W. Chan, *Science* **305**, 1941 (2004)
3. J. Day, J. Beamish, *Nature* **450**, 853 (2007)
4. M.W. Ray, R.B. Hallock, *Phys. Rev. Lett.* **100**, 235301 (2008)
5. X. Lin, A.C. Clark, Z.G. Cheng, M.H.W. Chan, *Phys. Rev. Lett.* **102**, 125302 (2009)
6. D.E. Galli, L. Reatto, *J. Phys. Soc. J.* **77**, 111010 (2008)
7. S. Balibar, F. Caupin, *J. Phys. Condens. Matter* **20**, 173201 (2008)
8. J. Saunders, *Science* **324**, 601 (2009)
9. G. Benedek, F. Dalfovo, R. Grisenti, M. Kász, J.P. Toennies, *Phys. Rev. Lett.* **95**, 095301 (2005)
10. G. Benedek, R. Grisenti, J.P. Toennies, F. Dalfovo, *J. Electron. Spectrosc. Relat. Phenom.* **129**, 201 (2003)
11. National Aperture, Inc, 16 Northwestern Drive, Salem, NH 03079 USA
12. Kistler Instruments (8408 Winterthur, Switzerland) high pressure quartz sensor type 601A with charge amplifier model 5015A
13. Kistler Instruments (8408 Winterthur, Switzerland) piezoresistive absolute pressure sensor type 4073A100 and piezoresistive amplifier model 4601A
14. E.R. Grilly, *J. Low Temp. Phys.* **11**, 33 (1972)
15. I. Iwasa, K. Araki, H. Suzuki *J. Phys. Soc. Jpn* **46**, 1119 (1979)
16. c_L was set equal to the value of c_{33} from ultrasonic measurements by R.H. Crepeau, O. Heybey, D.M. Lee, S.A. Strauss, *Phys. Rev. A* **3**, 1162 (1971)
17. B.N.J. Persson, *Sliding Friction* (Springer, 1998), p. 150, Figure 7.39(f)
18. G. Benedek, A. Kalinin, P. Nieto, J.P. Toennies, to be published